ISSN: 2579-5821 (Print)
ISSN: 2579-5546 (Online)
URL address: http://journal.unhas.ac.id/index.php/geocelebes
DOI: 10.70561/geocelebes.v10i2.53132

Jurnal Geocelebes Vol. 10 No. 2, October 2026, 443 – 470

Projected Changes in Rainy Season Onset, Retreat, and Duration over the Brantas Watershed Using Downscaled CMIP6 Climate Models

Gilang Aulia Herlambang, Lalu Muhamad Jaelani

Geomatics Engineering, Institut Teknologi Sepuluh Nopember, Surabaya 60111, Indonesia.

Corresponding author. Email: gilangauliaherlambang@gmail.com

Manuscript received: 31 July 2026; Received in revised form: 26 October 2026; Accepted: 31 October 2026

Abstract

This study evaluates projected changes in rainy-season onset, retreat, duration, and peak timing across the Brantas Watershed, Indonesia, using five downscaled CMIP6 climate models under SSP2-4.5 and SSP5-8.5 scenarios. Daily precipitation was downscaled to approximately 0.05° resolution using the BCCAQ method. Rainy-season characteristics were determined using the Indonesian Agency for Meteorology, Climatology, and Geophysics (BMKG) 10-daily criteria and compared with the accumulated rainfall anomaly method. Historical validation against rain-gauge observations (2000–2014) showed generally better performance for the BMKG method, with onset and retreat RMSE values of approximately 12–22 days. Projections indicated an advance in rainy-season onset of approximately 43–53 days and an increase in duration of 41–58 days relative to the 1981–2014 baseline. Retreat timing remained relatively stable under the BMKG method. However, a statistically significant increasing trend in duration was identified only under SSP5-8.5. The anomaly method showed smaller and less consistent duration changes, ranging from −7.9 to +8.5 days. Peak rainfall timing tended to occur earlier, particularly under SSP5-8.5, although substantial interannual variability persisted. These findings highlight the influence of seasonal determination methods on projected rainfall characteristics and provide relevant information for agricultural planning and water-resource management.

Keywords: BCCAQ downscaling; Brantas Watershed; CMIP6; SSP scenarios; Rainy season.

Citation: Herlambang, G. A., & Jaelani, L. M. (2026). Projected Changes in Rainy Season Onset, Retreat, and Duration over the Brantas Watershed Using Downscaled CMIP6 Climate Models. *Jurnal Geocelebes*, 10(2): 443–470, doi: 10.70561/geocelebes.v10i2.53132

Introduction

Climate change is widely acknowledged as a paramount environmental crisis of the twenty-first century, with documented and anticipated consequences for ecosystem stability, food security, water resources, and global economic resilience (IPCC, 2023). The Intergovernmental Panel on Climate Change (IPCC) assessed global mean surface temperature in 2011–2020 as approximately 1.1°C above the 1850–1900 average; the 1.5°C warming level is projected to be reached in the near term under many assessed scenarios (IPCC, 2021; IPCC, 2023). Continued warming is expected to influence atmospheric circulation, precipitation variability, and hydroclimatic extremes, although the magnitude and direction of local precipitation changes differ among regions and models.

The effects of climate change are expected to be particularly noticeable in tropical regions, where climate systems are often more sensitive to external forcing. Indonesia, located within the Asian–Australian monsoon domain (Mulsandi et al., 2024), experiences precipitation variability that is strongly influenced by the interaction between monsoonal circulation, El Niño–Southern Oscillation (ENSO), and the Indian Ocean Dipole (IOD) (Supari et al., 2018, 2020; Kurniadi et al., 2023). These factors contribute to

© 2026 Dept. of Geophysics Hasanuddin University

considerable spatial and temporal heterogeneity in rainfall distribution across the archipelago (Kurniadi et al., 2023; Sudarman et al., 2024; Yulizar & Asdak, 2025). In addition to affecting total annual precipitation, climate change may also alter the seasonal characteristics of rainfall, including the timing of rainy season onset, cessation, and overall duration. Such changes are potentially important for agricultural planning, irrigation management, and adaptation strategies, as many agricultural systems remain highly dependent on seasonal rainfall patterns (Adriat et al., 2025; Shrestha et al., 2025). This highlights the need for localized climate assessments that can provide more detailed information for regions with high dependence on water resources.

The Brantas Watershed in East Java, Indonesia, is an important river basin that supports agricultural production, water supply, flood management, and hydropower generation (BBWS Brantas, 2011; Wiwoho et al., 2023). Seasonal rainfall is closely linked to water availability and agricultural activities, making changes in rainy-season timing and duration important considerations for watershed management (Kwawuvi et al., 2022; Long et al., 2023). Studies in the Oti River Basin in West Africa and the Xiang River Basin in China have demonstrated that rainy-season onset, cessation, and duration can vary over time, with potential implications for agricultural planning and water management (Kwawuvi et al., 2022; Long et al., 2023).

Furthermore, CMIP6-based projections indicate that future changes in rainy-season onset, retreat, and duration may differ across monsoon regions and emission scenarios (Moon & Ha, 2020; Taguela et al., 2026). These findings highlight the importance of assessing seasonal rainfall timing alongside changes in precipitation amounts when investigating future climate impacts on water resources and agricultural systems (Kwawuvi et al., 2022; Moon & Ha, 2020). In the Brantas Watershed, previous research has examined rainfall variability, agricultural productivity, and future precipitation projections (Wiwoho et al., 2023, 2025; Herlambang & Jaelani, 2026). Further investigation of projected changes in rainy-season onset, retreat, duration, and peak timing can complement these studies by providing additional information on the seasonal distribution of rainfall relevant to water resource management and climate adaptation.

For future climate projections, the Coupled Model Intercomparison Project Phase 6 (CMIP6) provides a widely used set of global climate model (GCM) simulations under various Shared Socioeconomic Pathways (SSPs) (Eyring et al., 2016; O'Neill et al., 2016; Tebaldi et al., 2021). However, GCM outputs are generally produced at coarse spatial resolutions and may contain systematic biases that limit their direct application for local-scale studies, especially in tropical areas where precipitation processes are complex and highly variable (Chen et al., 2021; IPCC, 2021). To address this limitation, downscaling and bias correction techniques are often applied to improve the representativeness of GCM data at regional and local levels (Gebrechorkos et al., 2023; Raghavan et al., 2018). One such method is the Bias Correction Constructed Analogues with Quantile Mapping Reordering (BCCAQ), which combines the spatial pattern preservation capability of Constructed Analogues with the statistical distribution correction of Quantile Mapping (Cannon et al., 2015; Werner & Cannon, 2016). Studies have shown that BCCAQ effectively reduces systematic biases and enhances the representation of precipitation variability and extreme events in downscaled climate projections (Werner & Cannon, 2016; Gebrechorkos et al., 2023). The application of bias correction and

© 2026 Dept. of Geophysics Hasanuddin University

downscaling is now considered a necessary step for generating climate information suitable for local impact assessments (Lafferty & Sriver, 2023).

In recent years, BCCAQ-downscaled CMIP6 data have been increasingly employed in climate-related studies in Indonesia, including analyses of temperature changes, rainfall characteristics, extreme climate indices, and hydrological responses (Kurniadi et al., 2023, 2024; Yulizar & Asdak, 2025; Herlambang & Jaelani, 2026). However, most of these studies have concentrated on changes in the magnitude of climate variables, while less attention has been given to the seasonal timing of rainfall (onset, retreat, and duration) at watershed scales. For instance, while Hariadi et al. (2022) evaluated the onset and cessation of the rainy season across Southeast Asia, their analysis was conducted at a broad regional scale rather than at a specific watershed scale.

The novelty of this study lies in its comprehensive watershed-scale assessment of rainy season timing in the Brantas Watershed. Unlike previous regional studies that focused primarily on precipitation magnitudes, this study specifically quantifies the projected shifts in onset, retreat, duration, and peak timing at a high spatial resolution (~5.5 km) using newly BCCAQ CMIP6 data. Furthermore, this study provides a critical methodological comparison between the operational BMKG threshold method and the international cumulative anomaly method, offering a robust framework for assessing seasonal rainfall shifts in complex tropical terrains.

This study investigates projected changes in rainy-season characteristics across the Brantas Watershed using BCCAQ-downscaled CMIP6 precipitation data. The specific objectives are to: (1) evaluate the performance of five CMIP6 climate models against observational precipitation data using statistical metrics; (2) quantify projected changes in rainy-season onset, retreat, duration, and peak timing under the SSP2-4.5 and SSP5-8.5 scenarios across the near-term (2015–2040), mid-term (2041–2070), and long-term (2071–2099) periods relative to the 1981–2014 baseline; and (3) compare the projected changes in rainy-season onset, retreat, and duration derived using the BMKG and rainfall-anomaly methods, considering their temporal trends and spatial variability. The findings are expected to support climate adaptation planning, water resource management, and agricultural scheduling in the Brantas Watershed. It should be noted that the scope of this study is limited to the evaluated GCMs, the two selected seasonal determination methods, and the specific projection periods, which may not fully capture all possible future climate trajectories.

Materials and Methods

Study Area

The Brantas Watershed (DAS Brantas) is located in East Java Province, Indonesia, between approximately 111°30′–112°55′ East Longitude and 7°01′–8°15′ South Latitude, with a catchment area of about 11,800 km² and a main river length of approximately 320 km (BBWS Brantas, 2011; Wiwoho et al., 2023). The geographical location and spatial extent of the study area are presented in Figure 1. The upstream portion of the watershed is situated in the mountainous region of Batu City and Malang Regency, while the river flows through the central area, which is predominantly characterized by agricultural land and settlements, before discharging into the Madura Strait. The watershed is supported by several multipurpose reservoirs, including Sutami (Karangkates), Lahor, Selorejo, Wlingi, and Lodoyo, which serve functions such as flood control, raw water supply, irrigation, and hydropower generation (BBWS

© 2026 Dept. of Geophysics Hasanuddin University

Brantas, 2011). The topographic conditions of the Brantas Watershed vary considerably, ranging from volcanic mountainous areas in the upstream section to lowland coastal plains in the downstream section. These variations contribute to spatial differences in rainfall distribution across the watershed, suggesting that an assessment of changes in rainy season characteristics should consider spatial approaches to better represent the heterogeneity of precipitation patterns within the watershed.

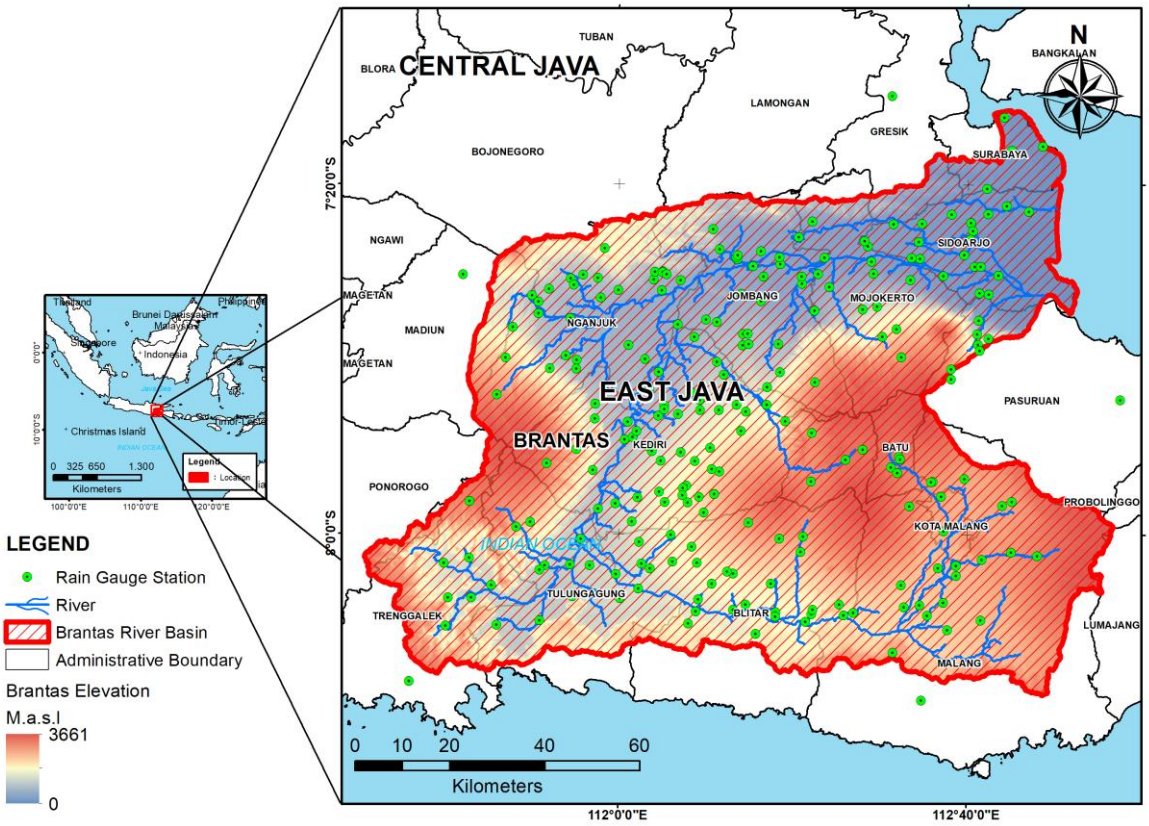


Figure 1. Geographic location and spatial characteristics of the Brantas Watershed, East Java, Indonesia, showing the watershed boundary, digital elevation model (DEM), and spatial distribution of 216 rain gauges within the watershed, selected from 221 available stations.

Data

Observational Precipitation Data

Two precipitation datasets were utilized in this study. The first was the Climate Hazards Group InfraRed Precipitation with Station data version 2.0 (CHIRPS v2.0) (Funk et al., 2015), available at a spatial resolution of 0.05o (approx. 5.5 km) and a daily temporal resolution. CHIRPS v2.0 was employed as the observational reference (training target) for calibrating and downscaling the CMIP6 climate models using the BCCAQ method over the baseline period of 1981–2014. Although CHIRPS exhibits known limitations in capturing exact daily rainfall timing and fine-scale orographic precipitation (Rahmawati & Lubczynski, 2018; Wiwoho et al., 2021), aggregating daily estimates into dasarian (10-day) totals substantially mitigates daily temporal noise and uncertainties (Dinku et al., 2018; Wiwoho et al., 2021), rendering it suitable for robust rainy-season onset and retreat detection across regional domains. CHIRPS has also been evaluated against rain-gauge observations in Indonesia, including the Brantas Watershed (Ferijal et al., 2025; Wiwoho et al., 2021), and in other regions (Bai et al., 2018; Dinku et al., 2018; Paredes-Trejo et al., 2017).

© 2026 Dept. of Geophysics Hasanuddin University

The second dataset comprised daily rain-gauge observations provided by the Indonesian Agency for Meteorology, Climatology, and Geophysics (BMKG) and the Department of Public Works and Water Resources (PU SDA) of East Java Province for the validation sub-period of 2000–2014. A total of 221 rain-gauge stations were available, of which 216 were located within the Brantas Watershed and met the quality-control criteria. The remaining five stations were located outside the watershed boundary and were excluded from the watershed-scale validation. Quality-control procedures included screening for non-physical values, identifying prolonged frozen values, and enforcing a minimum data-completeness threshold of 85% across the 2000–2014 period.

While CHIRPS drove the BCCAQ calibration process, the independent rain-gauge observations (restricted to 2000–2014) served strictly as an external validation dataset to evaluate the performance of the downscaled precipitation estimates. Although complete independence between gridded products and station data can be challenging due to station incorporation in CHIRPS generation, this gauge-based evaluation provides a rigorous assessment of how closely the BCCAQ-adjusted outputs reproduce observed station-scale variability across the watershed.

CMIP6 Climate Model Data and SSP Scenarios

Projected precipitation data were obtained from the Coupled Model Intercomparison Project Phase 6 (CMIP6) via the Earth System Grid Federation (ESGF) portal. Five GCMs MIROC-ES2L, EC-Earth3-Veg-LR, IPSL-CM6A-LR, NorESM2-MM, and GFDL-ESM4 were selected based on previous regional precipitation evaluations across Southeast Asia and Indonesia. Specifically, MIROC-ES2L demonstrated strong performance over the Brantas River Basin (Herlambang & Jaelani, 2026), EC-Earth3-Veg-LR, IPSL-CM6A-LR, and GFDL-ESM4 were identified among the top-performing models for reproducing precipitation dynamics and seasonal cycles across Southeast Asia (Iqbal et al., 2021; Liu et al., 2023; Pimonsree et al., 2023), and NorESM2-MM showed robust skill across regional evaluations (Kurniadi et al., 2023; Liu et al., 2022). Retaining these five structurally independent models provides a manageable multi-model ensemble to account for structural uncertainty and capture differences in projected climate responses (Tebaldi et al., 2021). The detailed specifications of the five selected CMIP6 models, including their development institutions and native spatial resolutions, are summarized in Table 1.

Table 1. Specifications of the five CMIP6 Global Climate Models (GCMs) used in this study.

Model	Institution (Country)	Native Resolution (Lat × Lon)	Reference
EC-Earth3-Veg-LR	EC-Earth Consortium (Europe)	~1.0° × 1.0°	Döscher et al. (2022)
GFDL-ESM4	NOAA-GFDL (USA)	~1.0° × 1.25°	Dunne et al. (2020)
IPSL-CM6A-LR	IPSL (France)	~1.26° × 2.5°	Boucher et al. (2020)
MIROC-ES2L	MIROC (Japan)	~2.8° × 2.8°	Hajima et al. (2020)
NorESM2-MM	NCC (Norway)	~1.0° × 1.0°	Seland et al. (2020)

Rather than re-using existing downscaled outputs, raw daily GCM series were newly downscaled in this study to a 0.05° spatial resolution over the Brantas Watershed via the BCCAQ method. To prevent circular reasoning, the initial model selection based on macro-climatological skill is strictly separated from the validation in Section 2.4, which independently evaluates these newly downscaled products against daily rain-gauge observations across higher-order daily variability, extreme

© 2026 Dept. of Geophysics Hasanuddin University

precipitation indices, and rainy-season onset/ retreat dynamics.

The historical baseline covers 1981–2014, corresponding to the period used to calibrate the BCCAQ method against CHIRPS v2.0 precipitation data. In contrast, validation against ground-based daily rainfall observations is restricted to the 2000–2014 sub-period, aligning with station data availability and quality control criteria.

Future projections were extracted under two Shared Socioeconomic Pathways: SSP2-4.5, describing a "middle-of-the-road" pathway, and SSP5-8.5, representing a fossil-fuel-intensive, high-emissions pathway (Riahi et al., 2017). Together, they provide a robust foundation for assessing precipitation changes across a moderate-to-high range of future forcing scenarios (IPCC, 2021). Future changes are evaluated over three distinct 30-year time horizons: 2015–2040 (near-term), 2041–2070 (mid-century), and 2071–2099 (end-century). These time horizons enable a comprehensive evaluation of progressive climate shifts throughout the twenty-first century, while internal climate variability is acknowledged as a potential source of uncertainty in near-term projections.

BCCAQ Statistical Downscaling

The native spatial resolution of CMIP6 GCM outputs (100–250 km) is too coarse to capture fine-scale precipitation variability across the topographically complex Brantas Watershed. To bridge this spatial scale gap, raw daily precipitation series from the five selected CMIP6 models were downscaled using the Bias Correction/ Constructed Analogues with Quantile Mapping Reordering (BCCAQ) method (Werner & Cannon, 2016). BCCAQ is a hybrid statistical downscaling technique that integrates Constructed Analogues (CA) spatial downscaling with Quantile Delta Mapping (QDM) bias correction (Cannon et al., 2015).

Rather than performing daily-scale bias correction, the BCCAQ algorithm executes a multi-step integration process:

1. Bias Correction: Raw daily GCM outputs at their native resolutions are first bias-corrected against a coarse-aggregated observational reference using QDM (Cannon et al., 2015). QDM adjusts historical and future GCM quantiles while explicitly preserving the model's projected relative change signals across all quantiles, ensuring that climate change signals in extreme values are retained.
2. Constructed Analogues (CA) Spatial Downscaling: Daily large-scale atmospheric patterns from the GCM are constructed as optimal linear combinations of N analog days selected from the historical observational record, downscaling the spatial pattern to the fine observational grid (Werner & Cannon, 2016).
3. Quantile Mapping Reordering: To preserve spatial co-variability and prevent artificial variance reduction in extreme events, high-resolution QDM outputs at each target grid cell are reordered based on the rank structure derived from the CA spatial patterns (Werner & Cannon, 2016).

Downscaling was executed using CHIRPS v2.0 daily precipitation data at its native spatial resolution of ~0.05° (5x5 km) as the observational target dataset over the 34-year calibration period (1981–2014). Key algorithmic parameters were configured as follows (Cannon et al., 2015; Werner & Cannon, 2016):

- Wet-day threshold: Set to 0.1 mm/day to differentiate wet and dry states and avoid trace-precipitation bias during quantile mapping.
- Number of analogues (N): Configured to N = 30 historical analog days to construct spatial patterns while

© 2026 Dept. of Geophysics Hasanuddin University

preventing over-smoothing of local orographic extremes.
- QDM distribution: Empirical cumulative distribution functions (eCDFs) were constructed non-parametrically using 100 quantiles evaluated across a rolling 31-day centered window to account for seasonal non-stationarity without parametric distribution assumptions.

The resulting dataset provides continuous, high-resolution (~0.05º, 5.5 km) daily precipitation projections across the Brantas Watershed for both the historical baseline (1981–2014) and future projection horizons (2015–2100) under SSP2-4.5 and SSP5-8.5.

GCM Performance Evaluation and Model Selection

To assess the fidelity of the downscaled climate simulations over the Brantas Watershed, outputs from all five downscaled CMIP6 models (MIROC-ES2L, EC-Earth3-Veg-LR, IPSL-CM6A-LR, NorESM2-MM, and GFDL-ESM4) were evaluated against observed ground-based daily precipitation during the independent historical sub-period (2000–2014). Observational data were obtained from 216 rain-gauge stations located within the Brantas Watershed that met the quality-control criteria. Although 221 stations were initially available, five stations located outside the watershed boundary were excluded from the validation. The selected station records were spatially interpolated using Ordinary Kriging to produce reference precipitation fields at a 0.05° grid resolution for comparison with the downscaled CMIP6 outputs. Because the BCCAQ downscaling procedure was calibrated exclusively against CHIRPS v2.0 over 1981–2014, evaluating the downscaled outputs against station-interpolated surfaces over 2000–2014 serves as an independent split-sample validation.

Model performance was evaluated across both daily rainy-season characteristics. First, general model performance was quantified using four statistical metrics: Correlation Coefficient (CC) for temporal coherence, Root Mean Square Error (RMSE) and Percent Bias (PBias) for magnitude deviations, and Standard Deviation Ratio (StdRatio) for spatial variability (Prasetya et al., 2026). These metrics were integrated using Taylor diagrams and heatmaps to visually compare spatial and temporal performance across models. Second, to rigorously test the daily-scale performance of the BCCAQ outputs, historical simulations were explicitly evaluated against observations for rainy-season dynamics, including onset date, retreat date, duration, and peak rainfall intensity, following previous evaluations of simulated rainy-season onset and cessation (Dunning et al., 2017; Hariadi et al., 2022).

Rather than using model rankings to assign differential weights or eliminate lower-ranked models, all five GCMs were retained to construct an unweighted multi-model ensemble based on the simple arithmetic mean. This approach preserves the representation of structural uncertainty and inter-model spread across future climate projections, aligning with multi-metric evaluation benchmarking frameworks for regional climate change studies in Southeast Asia (Gupta et al., 2025; Iqbal et al., 2021; Pimonsree et al., 2023; Prasetya et al., 2026; Shakeel et al., 2025; Zabihi & Ahmadi, 2024).

Determination of Rainy Season Onset, Retreat, and Duration

The rainy season characteristics in this study were defined using three main parameters: onset, retreat (or cessation), and rainy season duration, which collectively describe the timing, length, and variability of the rainy season in a given region (Bombardi et al., 2020). Various methods have been developed in

© 2026 Dept. of Geophysics Hasanuddin University

the international literature to determine these parameters, ranging from cumulative rainfall threshold approaches, two-phase regression analysis on cumulative rainfall data, to wavelet transform-based methods, each with different characteristics and levels of sensitivity to noise in precipitation data (Bombardi et al., 2020). This study combined two complementary approaches: the operational 10-daily (dasarian) criteria established by the Indonesian Agency for Meteorology, Climatology, and Geophysics (BMKG) as the primary method, which is operationally relevant in Indonesia, and the accumulated rainfall anomaly approach, which is commonly used in international CMIP6 scientific literature, as a comparative method to strengthen the scientific validity of the results.

BMKG 10-Daily (Dasarian) Criteria

The primary method used in this study follows the operational criteria established by the Agency for Meteorology, Climatology, and Geophysics of Indonesia (BMKG, 2022), which divide each month into three 10-day periods (dasarian): Dasarian I (days 1–10), Dasarian II (days 11–20), and Dasarian III (days 21 to the end of the month).

To avoid truncating the natural wet season of Indonesia which is dominated by the Asian winter monsoon and typically spans from late November through April across the calendar year boundary (BMKG, 2022) the search window for determining seasonal characteristics was set according to the hydrological year spanning from 1 August to 31 July of the following year. Within this defined annual search window, the rainy season parameters were calculated as follows:

a. Rainy season onset is defined as the first dasarian in which the 10-day rainfall total reaches or exceeds 50 mm, followed by two subsequent dasarians that also meet this criterion, thus constituting three consecutive dasarians with rainfall 50 mm (BMKG, 2022).
b. Rainy season retreat (marking the onset of the dry season) is defined as the first dasarian in which the 10-day rainfall total falls below 50 mm, followed by two subsequent dasarians that also remain below this threshold.
c. Rainy season duration is calculated as the total number of dasarians between onset and retreat.
d. Rainy season peak is determined as the period of three consecutive dasarians with the highest accumulated rainfall within a single seasonal year.

The 10-daily (dasarian) criteria were selected because they represent the official operational standard used by BMKG for seasonal forecasting and planting calendar determination in Indonesia (BMKG, 2022). Consequently, the results are directly relevant to agricultural and water resource management frameworks in the Brantas Watershed.

Accumulated Rainfall Anomaly Method (Complementary Approach)

As a comparative method, this study also applied the accumulated rainfall anomaly approach developed by Liebmann et al. (2007), which has been widely adopted in regional climate studies and precipitation evaluations across Indonesia and Southeast Asia (Hariadi et al., 2022; Dunning et al., 2018). This method calculates the accumulation of daily rainfall anomalies relative to the mean annual daily rainfall, with the general formulation given in Equation (1) (Liebmann et al., 2007; Dunning et al., 2018):

$$A(t) = \sum_{n=1}^{t} (R_n - \bar{R}) \qquad (1)$$

where $A(t)$ is the accumulated anomaly value on day t, $R(n)$ is the daily rainfall on day n, and $\bar{R}$ is the mean rainfall across the hydrological year (Liebmann et al., 2007; Dunning et al., 2018; Hariadi et al., 2022).

© 2026 Dept. of Geophysics Hasanuddin University

To avoid splitting the continuous wet season over the Brantas Watershed across calendar year boundaries, the accumulation calculation was executed on a hydrological year basis starting on 1 August corresponding to the climatologically driest period of the year and extending through 31 July of the following year.

Within this seasonal-year frame, rainy season onset is defined as the day when $A(t)$ reaches its absolute minimum value, marking the transition from dry-season conditions to daily rainfall consistently exceeding the annual mean. Conversely, rainy season retreat is defined as the day when $A(t)$ reaches its absolute maximum value, representing the transition back to conditions below the annual mean (Liebmann et al., 2007; Dunning et al., 2018). Rainy season duration is subsequently determined as the total number of days elapsed between the identified onset and retreat dates.

Trend and Statistical Significance Analysis

Temporal trends in rainy-season characteristics were assessed using the modified Mann–Kendall (MMK) test, which accounts for serial autocorrelation in climate time series (Hamed & Rao, 1998). Trend magnitudes were estimated using Sen's slope estimator and expressed in days per decade. Statistical significance was initially evaluated at $p < 0.05$. For spatial analyses involving multiple grid cells, the false discovery rate (FDR) procedure of Benjamini & Hochberg (1995) was applied at a significance level of $\alpha = 0.10$ to account for multiple testing.

The inter-model signal-to-noise ratio (SNR) was calculated as the absolute ensemble-mean change divided by the standard deviation of changes across the five climate models. An SNR greater than 1 indicates that the magnitude of the ensemble-mean signal exceeds the inter-model standard deviation, whereas a lower value indicates greater relative inter-model uncertainty. SNR was interpreted as a measure of signal strength rather than as a statistical significance test.

Differences between future projection periods and the historical baseline were also assessed using Welch's t-test on the ensemble-mean annual time series for each grid cell. This test accommodates unequal variances between the two periods. Grid cells with fewer than five valid annual values in either comparison period were excluded. FDR-adjusted significance results were reported separately from temporal trend significance. Where insufficient valid baseline observations prevented a reliable comparison, the corresponding significance result was reported as not applicable (N/A).

Spatial Change Analysis

Changes in rainy season characteristics were analyzed by calculating the differences (anomalies) between onset, retreat, and rainy season duration values for each projection period (SSP2-4.5 and SSP5-8.5; near-term 2015–2040, mid-term 2041–2070, and long-term 2071–2099) relative to the climatological values of the historical period, for each grid cell across the entire Brantas Watershed. Changes in onset and retreat are expressed in days, with positive values indicating a delay (later occurrence) and negative values indicating an advance (earlier occurrence), while changes in duration are also expressed in days, with positive values indicating a lengthening and negative values indicating a shortening of the rainy season. The calculated results were then mapped spatially using Geographic Information System (GIS) software to identify patterns and areas with notable changes within the Brantas Watershed, thereby providing a comprehensive picture of the spatial variation in climate change impacts on rainy season characteristics across the study area.

© 2026 Dept. of Geophysics Hasanuddin University

Both approaches were applied consistently to the BCCAQ-downscaled precipitation data, for both the historical baseline period (1981–2014) and the projection periods under the SSP2-4.5 and SSP5-8.5 scenarios. Onset, retreat, and rainy season duration values were calculated for each grid pixel at the downscaled resolution across the entire Brantas Watershed and for each year within the simulation period. These values were then averaged across each time horizon (historical, near-term, mid-term, and long-term) to produce representative climatological values, ensemble means, and anomaly fields for each period.

Results and Discussion

Model Performance Evaluation of CMIP6 against Observational Data

Model validation was conducted by comparing the outputs of five CMIP6 global climate models namely MIROC-ES2L, EC-Earth3-Veg-LR, IPSL-CM6A-LR, NorESM2-MM, and GFDL-ESM4 against observational reference data. Model performance was evaluated using several statistical indicators, including Correlation Coefficient (CC, [-]), Root Mean Square Error (RMSE, mm/day), Percent Bias (PBias, %), Standard Deviation (Std Dev, mm/day), and Standard Deviation Ratio (StdRatio, [-]). In addition to numerical metric-based evaluation, the analysis was reinforced through visualization using heatmaps and Taylor diagrams to assess pattern agreement, variability, and the degree of deviation of each model relative to observations. The validation results are presented in Figures 2 and 3, with detailed numerical values provided in Table 2.



Figure 2. Comparison of the performance of five CMIP6 models based on statistical indicators evaluated against observational data.

Based on Figure 2, illustrates variations in model performance across the evaluated statistical indicators. Overall, each model exhibited distinct capabilities in representing historical precipitation characteristics over the Brantas Watershed. Among the five models, MIROC-ES2L showed relatively highest overall performance, as indicated by the lowest RMSE (3.17 mm/day) and the highest correlation coefficient (CC = 0.79). The lower error metric indicates closer agreement between model simulations and observations, while the higher correlation demonstrates a strong ability to capture observed precipitation variability patterns. Furthermore, a PBias value of -0.94% indicates minimal systematic bias, while a

© 2026 Dept. of Geophysics Hasanuddin University

StdRatio of 1.10 effectively reproduces the amplitude of observed variability.

The remaining four models also demonstrated competitive performance and complementary strengths in representing regional climate features. GFDL-ESM4 exhibited strong fidelity with a low error metric (RMSE = 3.28 mm/day), a high correlation coefficient (CC = 0.75), a near-unity standard deviation ratio (StdRatio = 1.03), and a slight positive bias (PBias = 0.86%). NorESM2-MM and EC-Earth3-Veg-LR produced comparable error ranges (RMSE of 3.36 mm/day and 3.49 mm/day; CC of 0.76 and 0.74, respectively), with EC-Earth3-Veg-LR displaying a slight dry bias (PBias = -4.34%) and NorESM2-MM showing a moderate wet bias (PBias = 9.01%). IPSL-CM6A-LR presented a higher amplitude of simulated variability (StdRatio = 1.28) and a wet bias (PBias = 9.60%), yet retained a strong pattern correlation (CC = 0.76).

Overall, while the downscaled models demonstrated reasonable capability in capturing the mean state and seasonal variability under the BMKG threshold method, the evaluation results based on the heatmap were further reinforced by the Taylor diagram in Figure 3, which integrates information on correlation, standard deviation, and RMSE within a single spatial representation. Model positions closer to the observational reference point indicate higher levels of agreement, as they reflect a combination of good correlation, standard deviation close to that of observations, and smaller errors.

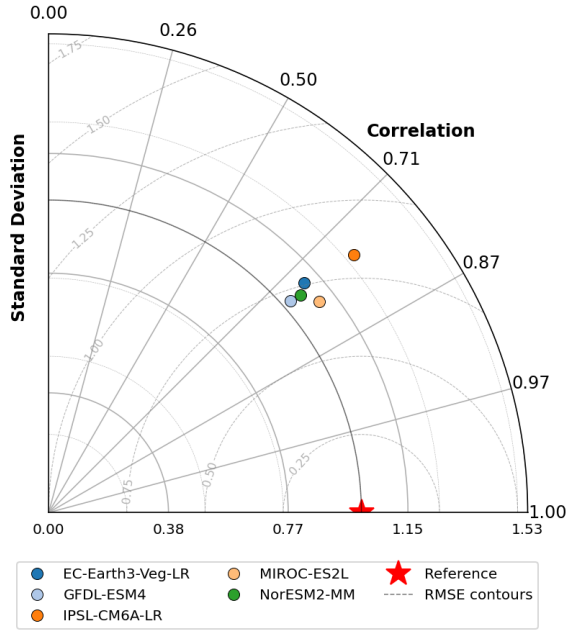


Figure 3. Taylor diagram evaluating the performance of five CMIP6 models against observational data.

In Figure 3, MIROC-ES2L is positioned relatively closest to the observational reference point, exhibiting the lowest RMSE (3.17 mm/day) and highest correlation coefficient (0.79) among the evaluated models. GFDL-ESM4 and NorESM2-MM occupied closely adjacent intermediate positions, reflecting strong correlation values and standard deviation ratios close to unity. Conversely, EC-Earth3-Veg-LR and IPSL-CM6A-LR exhibited slightly greater distances from the reference point, primarily driven by moderate dry/wet biases and higher standard deviation differences, while still maintaining high pattern correlation (CC = 0.74).

Overall, the results from the statistical metrics, heatmap, and Taylor diagram

© 2026 Dept. of Geophysics Hasanuddin University

consistently identified differences in capability among the CMIP6 models. MIROC-ES2L showed relatively exhibited the highest overall performance based on the combined evaluation of RMSE, CC, PBIAS, StdDev and StdRatio values, suggesting that this model achieved the highest level of agreement in representing historical precipitation characteristics over the Brantas Watershed. GFDL-ESM4 and NorESM2-MM also demonstrated robust performance, particularly in capturing variability amplitude with standard deviation ratios near unity (StdRatio = 1.03 and 1.06, respectively). The remaining models (EC-Earth3-Veg-LR and IPSL-CM6A-LR) provided complementary value by spanning the range of inter-model uncertainty, which is a key requirement of the multi-model ensemble framework.

Expanding this evaluation to seasonal transition dynamics, Table 2 provides a quantitative breakdown of historical onset, retreat, and duration evaluated against station observations for both the operational BMKG method and the ANOMALY method.

Table 2. Historical validation metrics of CMIP6 models against station observations (2000–2014) for BMKG and Anomaly methods.

Model	Method	Param	Obs Mean Days	Model Mean Days	Bias Days	Rmse Days	Spatial Corr
EC-Earth3-Veg-LR	BMKG	onset	126.2	132.4	6.2	13.8	0.74
		retreat	266.9	276.2	9.3	18	0.39
		duration	140.9	141.4	0.5	19.2	0.75
	ANOMALY	onset	109.1	203.2	94	94.4	0.5
		retreat	263	288.9	25.9	27.2	0.09
		duration	153.8	85.7	-68.1	68.9	0.52
GFDL-ESM4	BMKG	onset	125.8	144.3	18.5	21.5	0.76
		retreat	267	253.2	-13.8	20.4	0.46
		duration	141.4	107.6	-33.8	39	0.74
	ANOMALY	onset	107.7	120.1	12.4	14.1	0.68
		retreat	263.1	249.4	-13.7	15.4	0.17
		duration	155.4	129.2	-26.1	27.6	0.55
IPSL-CM6A-LR	BMKG	onset	126.2	124.4	-1.8	12	0.79
		retreat	266.9	255.8	-11.1	17.4	0.56
		duration	140.9	133.9	-6.9	17.1	0.85
	ANOMALY	onset	109.1	196.8	87.6	88	0.56
		retreat	263	289.1	26.2	27.6	0.12
		duration	153.8	92.3	-61.5	62.7	0.54
MIROC-ES2L	BMKG	onset	126.2	115.9	-10.4	14.8	0.78
		retreat	266.9	269	2.1	13.2	0.73
		duration	140.9	153	12.2	19.1	0.87
	ANOMALY	onset	109.1	200.4	91.3	91.6	0.53
		retreat	263	281.7	18.7	20.7	0.16
		duration	153.8	81.3	-72.5	73.3	0.52
NorESM2-MM	BMKG	onset	125.8	140.3	14.6	21.1	0.77
		retreat	267	255.7	-11.3	20.6	0.37
		duration	141.4	115	-26.4	31.4	0.82
	ANOMALY	onset	107.7	117.3	9.6	12.5	0.7
		retreat	263.1	251.1	-12	13.5	0.27
		duration	155.4	133.8	-21.6	23.6	0.61

Table 2 shows that model performance depended on both the seasonal parameter and the method used to identify it. The BMKG method generally produced stronger spatial correlations and lower errors for duration, whereas the Anomaly method performed comparatively well for onset and retreat in selected models. These results indicate that neither method consistently outperformed the other for

© 2026 Dept. of Geophysics Hasanuddin University

every model and parameter. RMSE values ranged from 12.0 to 21.5 days for onset, 13.2 to 20.6 days for retreat, and 17.1 to 39.0 days for duration. Spatial correlation coefficients reached 0.79 for onset, 0.73 for retreat, and 0.87 for duration. MIROC-ES2L and IPSL-CM6A-LR showed particularly strong spatial agreement for duration, with correlation coefficients of 0.87 and 0.85, respectively.

In contrast, the Anomaly method exhibited substantial errors for onset and duration in several models. Onset RMSE ranged from 12.5 to 94.4 days, while duration RMSE ranged from 23.6 to 73.3 days. Retreat RMSE was comparatively lower, ranging from 13.5 to 27.6 days. Spatial correlations for retreat were also generally weak, ranging from 0.09 to 0.27. These results indicate that the Anomaly method did not perform consistently across models and rainy-season parameters, particularly for onset and duration.

Given the different strengths and limitations of individual models, the five-model ensemble provides a basis for examining inter-model variability and structural uncertainty in future projections. However, the reliability of the resulting projections remains dependent on model performance, the seasonal-index method, and the consistency of the projected responses across models.

Temporal and Spatial Analysis of Changes in Rainy Season Characteristics under SSP2-4.5 and SSP5-8.5 Scenarios

To evaluate the response of rainy season characteristics to climate change, the analysis was conducted using both the BMKG method and the anomaly method, considering three main parameters: onset, retreat, and duration. The evaluation was carried out across three projection periods: near-term (2015–2040), mid-term (2041–2070), and far-term (2071–2099). The temporal statistical results were then combined with spatial distributions to identify patterns of change in rainy season characteristics under the SSP2-4.5 and SSP5-8.5 scenarios, as presented in Figure 4 and 5.

Based on the BMKG method mapping results (Figure 4), the changes in rainy season characteristics showed different responses between the SSP2-4.5 and SSP5-8.5 scenarios. Overall, the onset parameter exhibited a consistent advance under both scenarios, while the retreat parameter remained relatively stable. Consequently, the duration parameter showed a tendency to lengthen, primarily driven by the earlier onset rather than by changes in retreat timing.

For the onset parameter, ensemble median derived using the BMKG method indicated an earlier rainy-season onset in all three projection periods relative to the 1981–2014 baseline. Under SSP2-4.5, the median changes were −45.1 days in the near term, −50.3 days in the mid term, and −53.2 days in the long term. Under SSP5-8.5, the corresponding changes were −42.8, −45.1, and −45.3 days. These values describe the median projected changes and should not be interpreted as evidence of uniform changes across all grid cells or models.

The retreat parameter, in contrast, showed only small changes. Under SSP2-4.5, the median change ranged from +1.4 days (near-term) to −0.4 days (long-term), while under SSP5-8.5 it ranged from −8.9 days (near-term) to −5.6 days (long-term). These results suggest that the retreat timing of the rainy season is relatively insensitive to the emission scenario, at least as detected by the BMKG threshold criterion.

© 2026 Dept. of Geophysics Hasanuddin University

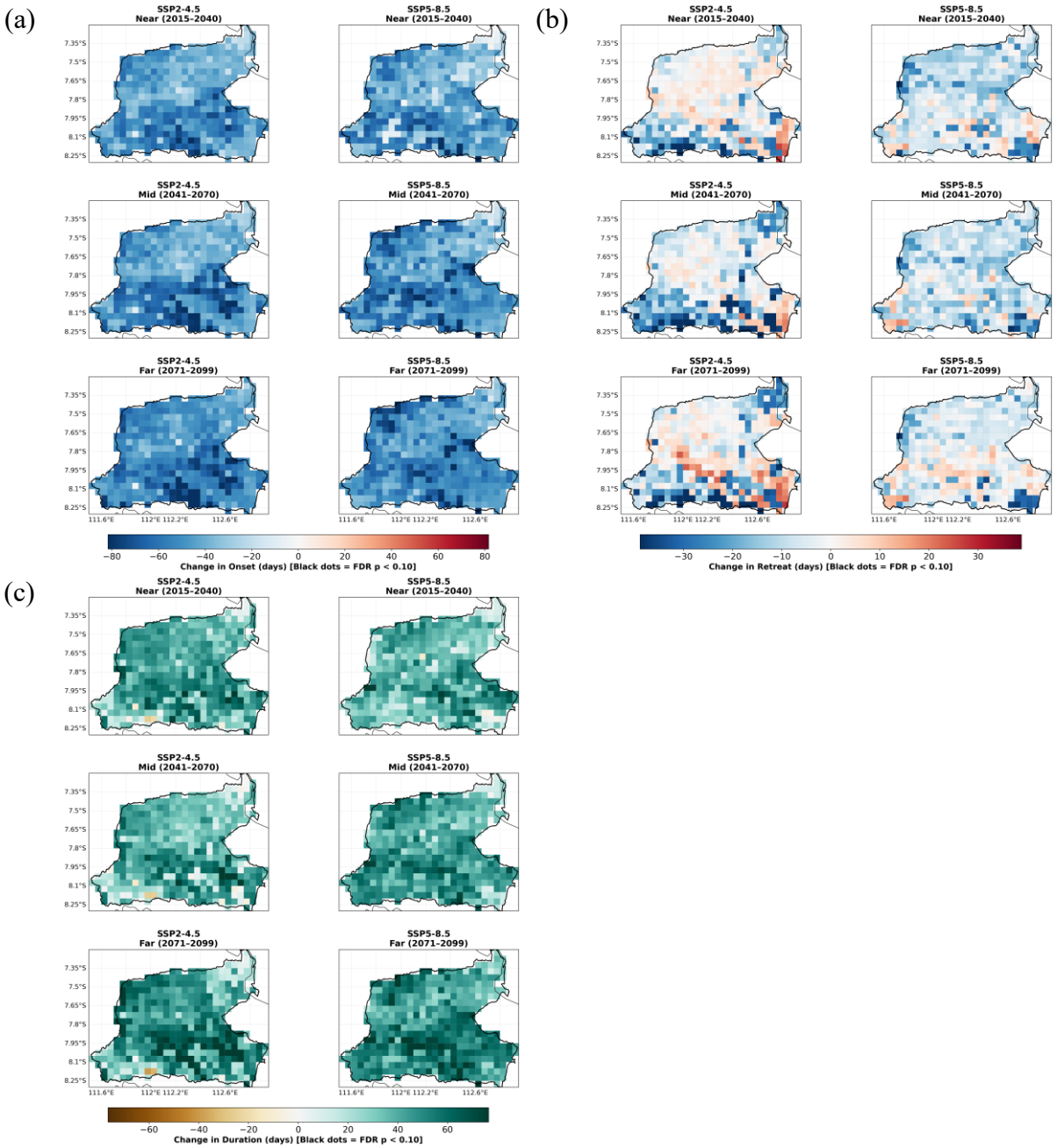


Figure 4. Spatial distribution of changes in (a) rainy season onset, (b) rainy season retreat, and (c) rainy season duration based on the BMKG method under SSP2-4.5 and SSP5-8.5 scenarios for the near-term (2015–2040), mid-term (2041–2070), and long-term (2071–2099) periods.

Changes in duration followed the pattern of onset and retreat. Under both scenarios, the rainy season duration lengthened substantially: +46.5 days (near-term), +41.0 days (mid-term), and +58.0 days (long-term) under SSP2-4.5; and +43.9, +44.7, and +51.1 days under SSP5-8.5. The spatial distribution (Figure 4c) showed widespread lengthening across the basin, consistent with the earlier onset identified in Figure 4a. Notably, the magnitude of duration lengthening was comparable between scenarios in the near-term and mid-term, but larger under SSP5-8.5 in the long-term period, suggesting an increasing response with higher emission forcing.

These values represent median changes relative to the 1981–2014 baseline for each projection period, rather than the temporal trend throughout 2015–2099. The period-specific median changes should be distinguished from the temporal trend estimates in Table 3. For the BMKG

© 2026 Dept. of Geophysics Hasanuddin University

method, duration showed a statistically significant increasing trend under SSP5-8.5 (Sen's slope = +2.573 days/decade, p = 0.0001), whereas the trend under SSP2-4.5 was not statistically significant (p = 0.0651). The Anomaly method yielded a contrasting significant decreasing trend under SSP5-8.5, highlighting the sensitivity of the projected duration response to the method used to define the rainy season

The anomaly method (Figure 5) quantified the magnitude of temporal deviation from the 1981–2014 climatology in days. In contrast to the BMKG method, which measures the absolute position of the rainy season, the anomaly method measures the relative shift of the seasonal cycle. The comparison between the two methods therefore provides complementary insight into the physical response of the rainy season to climate change.

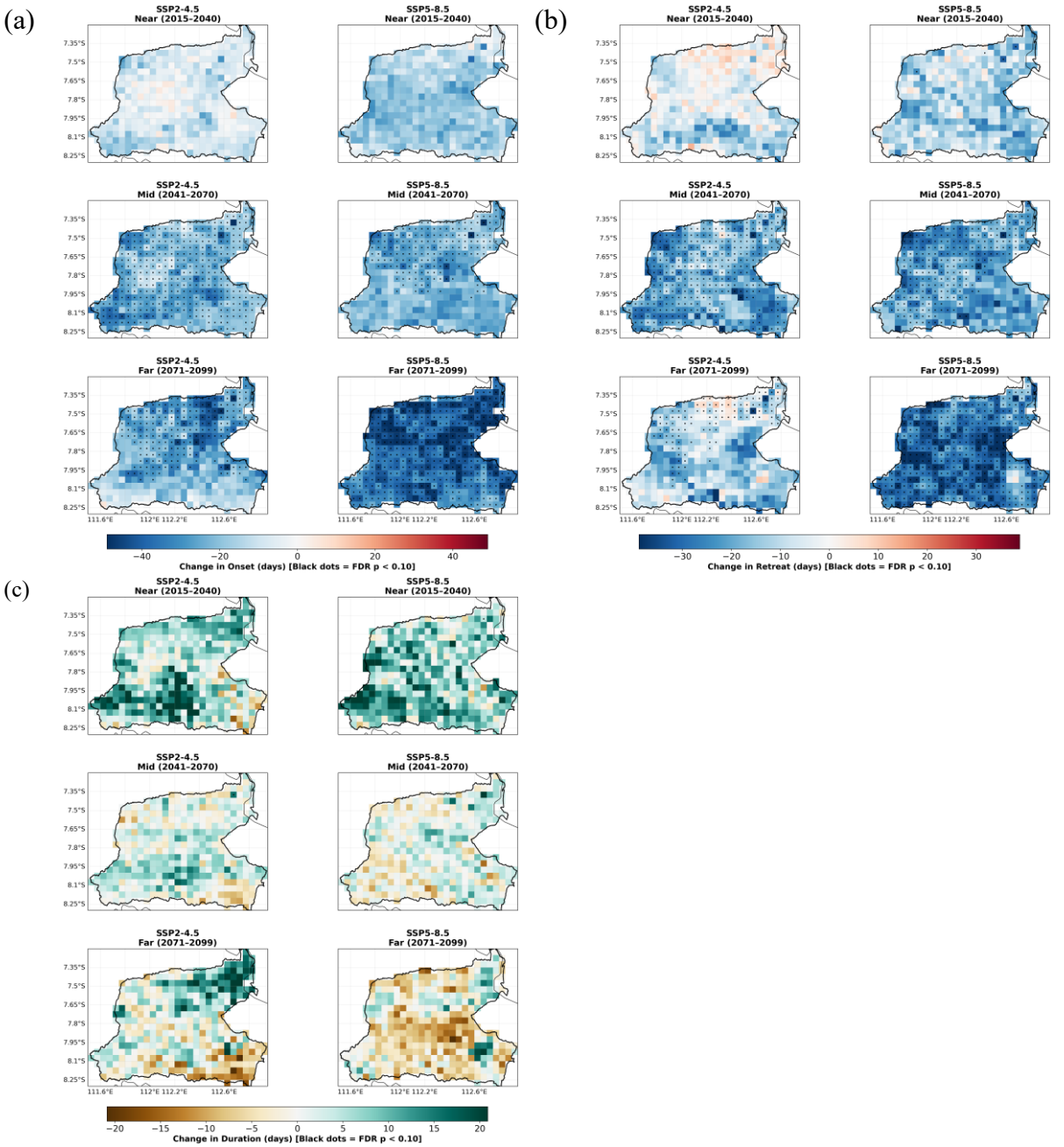


Figure 5. Spatial distribution of changes in (a) rainy season onset, (b) rainy season retreat, and (c) rainy season duration based on the anomaly method under SSP2-4.5 and SSP5-8.5 scenarios for the near-term (2015–2040), mid-term (2041–2070), and long-term (2071–2099) periods.

© 2026 Dept. of Geophysics Hasanuddin University

For onset, the Anomaly method indicated an earlier rainy-season onset under both scenarios, although the magnitude varied across projection periods. Under SSP2-4.5, the median onset changes were −6.1 days in the near-term period, −21.0 days in the mid-term period, and −23.9 days in the long-term period. Under SSP5-8.5, the corresponding changes were −20.2, −21.9, and −40.0 days. The inter-model signal-to-noise ratios ranged from 0.73 to 1.61 under SSP2-4.5 and from 1.95 to 4.06 under SSP5-8.5. These results indicate that the projected advance varied in magnitude and robustness across scenarios and periods

For retreat, the Anomaly method indicated an earlier retreat in all projection periods, in contrast to the relatively stable retreat timing derived using the BMKG method. Under SSP2-4.5, the median retreat changes were −5.4, −16.6, and −11.0 days in the near-term, mid-term, and long-term periods, respectively. Under SSP5-8.5, the corresponding changes were −11.6, −19.5, and −28.3 days. However, the signal-to-noise ratios varied considerably, ranging from 0.65 to 1.34 under SSP2-4.5 and from 0.74 to 2.77 under SSP5-8.5. Therefore, the direction of the median changes should be distinguished from the robustness of the projected response across models and grid cells.

For duration, the ANOMALY method produced small and inconsistent changes compared with the BMKG method. Under SSP2-4.5, the median duration changes were +2.2 days in the near-term period, +1.9 days in the mid-term period, and −3.6 days in the long-term period. Under SSP5-8.5, the corresponding changes were +8.5, −1.3, and −7.9 days. The signal-to-noise ratios ranged from 0.35 to 0.70 under SSP2-4.5 and from 0.07 to 0.14 under SSP5-8.5, indicating that the ensemble signal was generally weak relative to inter-model variability. The FDR-significant area was also negligible in most periods. Consequently, the Anomaly results do not support a robust conclusion regarding the direction or magnitude of future duration changes.

Table 3 summarizes the temporal trend estimates for rainy-season onset, retreat, and duration under SSP2-4.5 and SSP5-8.5 for both the BMKG and Anomaly methods. The table reports Sen's slope, the corresponding p-value, ensemble significance, and the dominant direction of change across models. In the BMKG method, onset and retreat are represented by their timing within the defined seasonal calendar, whereas duration represents the interval between these two transitions. In the Anomaly method, changes in timing and duration are expressed as differences from the 1981–2014 baseline. These quantities are interpreted separately because seasonal timing indices and duration have different meanings and should not be compared as equivalent measures.

Table 3. Summary of statistics and trend analysis for rainy season onset, retreat, & duration derived from the BMKG & anomaly methods under the SSP2-4.5 & SSP5-8.5 scenarios during the 2015–2099 projection period.

Method	Parameter	Scenario	Slope (days/decade)	Sig P	Ensemble Sig	Agreement
Anomaly	duration	SSP2-4.5	-0.3793	0.8954	No	Mostly decline
	onset	SSP2-4.5	-0.1196	0.0852	No	Mostly decline
	retreat	SSP2-4.5	-1.4943	0.0145	Yes	Mostly decline
BMKG	duration	SSP2-4.5	0.7228	0.0651	No	Mostly increase
	onset	SSP2-4.5	-0.6793	0.1771	No	Mostly decline
	retreat	SSP2-4.5	-0.8495	0.2121	No	Mostly decline
Anomaly	duration	SSP5-8.5	-3.3405	0.0142	Yes	Mostly decline
	onset	SSP5-8.5	-3.329	0.0279	Yes	Mostly decline
	retreat	SSP5-8.5	-0.9367	0.2449	No	Mostly decline
BMKG	duration	SSP5-8.5	2.573	0.0001	Yes	Consistent increase
	onset	SSP5-8.5	-0.2523	0.6636	No	Consistent decline
	retreat	SSP5-8.5	0.395	0.3763	No	Consistent increase

© 2026 Dept. of Geophysics Hasanuddin University

The modified Mann–Kendall trend analysis (Table 3) identified different temporal trends between the BMKG and Anomaly methods. Under the BMKG method, rainy-season duration under SSP5-8.5 showed a statistically significant increasing trend (Sen's slope = +2.57 days/decade, p = 0.0001), whereas onset and retreat showed no statistically significant trends at the 0.05 level. Under the Anomaly method, statistically significant trends were detected for onset under SSP5-8.5 (−3.329 days/decade, p = 0.0279), retreat under SSP2-4.5 (−1.4943 days/decade, p = 0.0145), and duration under SSP5-8.5 (−3.3405 days/decade, p = 0.0142). For anomaly-based duration under SSP5-8.5, the negative temporal trend indicates an overall tendency toward shorter rainy seasons during 2015–2099. However, the period-specific median changes relative to the 1981–2014 baseline were +8.5 days in the near term, −1.3 days in the mid term, and −7.9 days in the long term (Table 4). These values describe changes in separate projection periods, whereas the trend estimate represents the temporal tendency across the full projection period; therefore, the two results are not necessarily contradictory. Nevertheless, the low SNR values (0.07–0.14) and negligible FDR-significant area (0–0.3%) indicate that the anomaly-based duration signal is weak relative to inter-model variability and lacks substantial spatial significance. Consequently, the statistically significant temporal trend should not be interpreted as evidence of a robust, spatially consistent response across the watershed.

Tabel 4. Cross-method comparison of projected changes in rainy season onset, retreat, and duration (days) under SSP2-4.5 and SSP5-8.5.

Para-meter	Scenario	Period	BMKG Median	Anomaly Median	Diffe-rence	BMKG SNR	Anomaly SNR	BMKG FDR	Anomaly FDR
Onset	SSP2-4.5	2015-2040	-45.1	-6.1	-39	19.55	0.73	N/A	0
		2041-2070	-50.3	-21	-29.3	8.02	1.61	N/A	91
		2071-2099	-53.2	-23.9	-29.4	11.76	1.46	N/A	54.5
	SSP5-8.5	2015-2040	-42.8	-20.2	-22.7	1.45	1.95	N/A	0
		2041-2070	-45.1	-21.9	-23.3	2.4	4.06	N/A	46.5
		2071-2099	-45.3	-40	-5.3	2.54	2.32	N/A	97.7
Retreat	SSP2-4.5	2015-2040	1.4	-5.4	6.8	0.25	0.65	N/A	0
		2041-2070	-1.4	-16.6	15.2	0.64	1.34	N/A	85.1
		2071-2099	-0.4	-11	10.6	0.43	0.71	N/A	29.1
	SSP5-8.5	2015-2040	-8.9	-11.6	2.8	0.61	0.74	N/A	1
		2041-2070	-8.7	-19.5	10.8	0.91	2.77	N/A	65.8
		2071-2099	-5.6	-28.3	22.8	0.48	1.56	N/A	96.7
Duration	SSP2-4.5	2015-2040	46.5	2.2	44.3	2.49	0.53	N/A	0
		2041-2070	41	1.9	39.1	1.96	0.7	N/A	0.3
		2071-2099	58	-3.6	61.6	1.6	0.35	N/A	0
	SSP5-8.5	2015-2040	43.9	8.5	35.3	1.45	0.07	N/A	0.3
		2041-2070	44.7	-1.3	46	3.32	0.14	N/A	0
		2071-2099	51.1	-7.9	59	4.24	0.13	N/A	0

To compare the two methods, Table 4 presents the ensemble-median changes in onset, retreat, and duration for each scenario and projection period, together with the difference between methods, SNR values, and the percentage of grid cells showing FDR-significant changes where available. First, the advance of onset was consistently larger under the BMKG method (median −45 to −53 days) than under the anomaly method (median −6 to −40 days) for both scenarios and all periods. The difference may reflect the distinct ways in which the two methods identify seasonal transitions. The BMKG method is based on a predefined rainfall threshold, whereas the Anomaly method relies on deviations in

© 2026 Dept. of Geophysics Hasanuddin University

the accumulated rainfall cycle relative to the historical reference. Consequently, the methods may respond differently to changes in rainfall amount, timing, and within-season distribution. The present analysis does not independently establish which of these factors explains the observed differences.

Second, retreat showed opposite responses between the two methods. Under BMKG, retreat remained approximately stable (median change between −8.9 and +1.4 days) with low inter-model agreement (SNR = 0.25–0.91). Under the Anomaly method, the ensemble-median retreat change was negative in all projection periods, ranging from −5.4 to −28.3 days. For the long-term SSP5-8.5 period, 96.7% of grid cells were reported as FDR-significant. This spatial significance result should be interpreted separately from inter-model agreement and SNR, which describe different aspects of projection robustness.

Third, duration showed a substantial lengthening under the BMKG method (median +41 to +58 days) with moderate to high SNR (1.5–4.2). In contrast, the anomaly method showed only weak and inconsistent duration changes (median between −7.9 and +8.5 days) with very low SNR (0.07–0.70) and negligible FDR significance (< 1% in most periods). The larger signal under BMKG is consistent with the advance of onset being only partially offset by changes in retreat timing, whereas under the anomaly method, onset and retreat advance together, leaving duration approximately unchanged.

The projected changes varied spatially across the Brantas Watershed. At the ensemble-median level, both methods indicated an earlier onset, whereas retreat responses differed between methods and duration lengthening was evident primarily in the BMKG results. These basin-wide summaries do not imply uniform responses across all grid cells or models. The spatial patterns should therefore be interpreted together with the reported SNR and FDR results. However, attributing these variations to specific local drivers requires further analysis beyond the scope of this study.

Dynamics of Rainy Season Peak under Climate Change Scenarios

In addition to changes in rainy season onset and retreat, the timing of the rainy season peak represents an important indicator for understanding changes in the temporal distribution of rainfall within future climate systems. Shifts in the timing of peak rainfall may affect periods of maximum water availability, cropping patterns, and the risk of hydrometeorological events associated with seasonal rainfall intensity. Therefore, an analysis of the rainy season peak was conducted to evaluate changes in its spatial distribution and temporal variation under the SSP2-4.5 and SSP5-8.5 scenarios during the 2015–2099 projection period. The spatial distribution of rainy season peak timing is presented in Figure 6, while the temporal variation is shown in Figure 7.

Based on Figure 6, the spatial distribution of rainy season peak timing showed considerable regional variation under both scenarios. Overall, the northern part of the study area was predominantly characterized by earlier peak rainfall occurrence (approximately 100–140 days since 1 August, corresponding to mid-November to late December), while the southern region showed relatively later peak timing (approximately 160–200 days, corresponding to early January to mid-February). This north-to-south spatial gradient suggests that the distribution of maximum rainfall does not occur uniformly but rather follows the regional characteristics of the study area.

© 2026 Dept. of Geophysics Hasanuddin University

The differences in peak timing between regions indicate a clear spatial gradient. Areas located closer to the pathway of moist air mass inflow or those with more rapid atmospheric responses to seasonal transitions tended to experience earlier rainfall peaks, while other areas experienced delays due to differences in geographical conditions. However, identifying the specific atmospheric or topographic drivers behind this gradient requires further dedicated analysis.

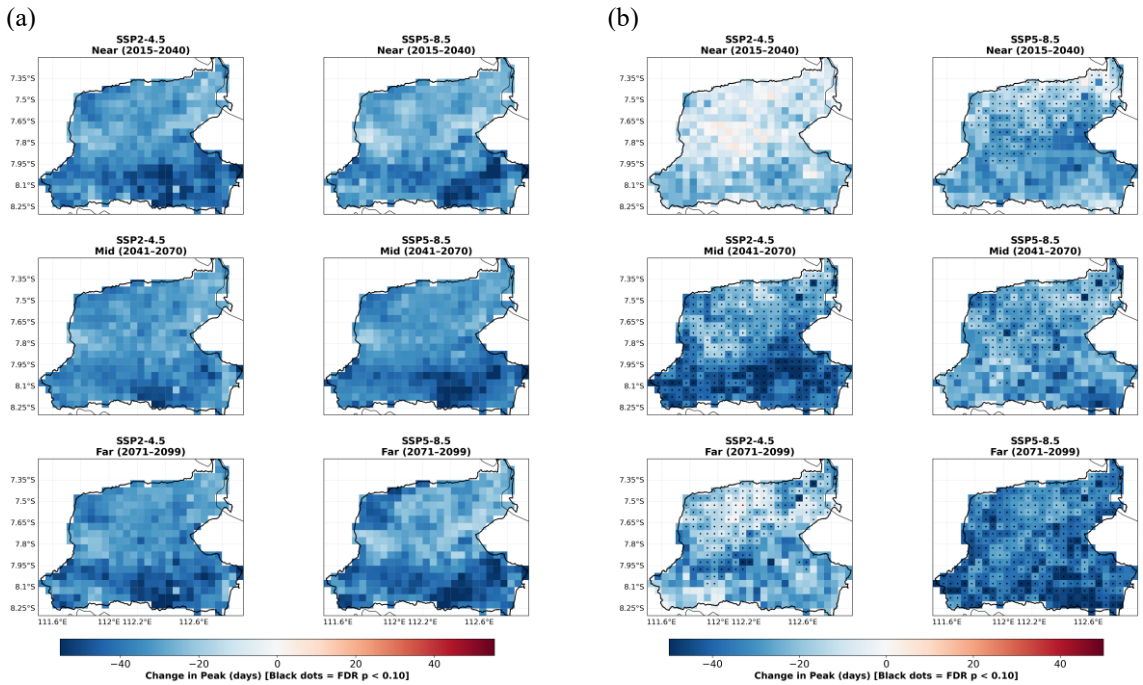


Figure 6. Spatial distribution of rainy season peak timing under SSP2-4.5 and SSP5-8.5 during 2015–2099 based on (a) BMKG and (b) anomaly methods.

Under the SSP2-4.5 scenario, most areas showed rainy season peak timing in the range of 100 to 150 days (mid-November to late December), with some southern areas reaching up to 200 days (mid-February). This distribution suggests that the spatial pattern of peak rainfall still generally maintained its overall characteristics, although local variations between areas were evident. This condition indicates that under the moderate emission scenario, changes in rainy season peak timing were more a matter of regional variation rather than widespread shifts in pattern.

Under SSP5-8.5, the mapped peak-timing index retained a broadly similar spatial pattern to that under SSP2-4.5, with values reaching approximately 210 days in parts of the southern and southeastern watershed. Because these maps show absolute timing rather than changes relative to the historical baseline, they do not establish whether peak rainfall becomes systematically later under the higher-emission scenario. These changes suggest differences in regional response to increased climate forcing. However, since the northern areas still maintained relatively earlier peak rainfall characteristics, the observed changes did not indicate a uniform shift across the entire region.

Spatially, these results suggest that higher emission scenarios do not directly lead to uniform changes in rainy season peak timing across all areas. Rather, the response of peak rainfall appears to remain controlled by a combination of large-scale climate changes and local factors that influence rainfall distribution. This differs from some other rainy season parameters, such as retreat and duration, which in

© 2026 Dept. of Geophysics Hasanuddin University

previous analyses showed more consistent changes across periods.

In addition to spatial distribution analysis, the temporal variation in rainy season peak timing during the 2015–2099 period is shown in Figure 7. The thin lines represent the annual values for each scenario, the thick lines represent the 5-year moving average to illustrate medium-term variations, and the dashed lines indicate the Sen's slope trend during the projection period. The y-axis represents the peak timing expressed in days since 1 August of the hydrological year (Day 0 = 1 August; for reference, Day 100 ≈ 9 November, Day 150 ≈ 29 December, and Day 200 ≈ 17 February).

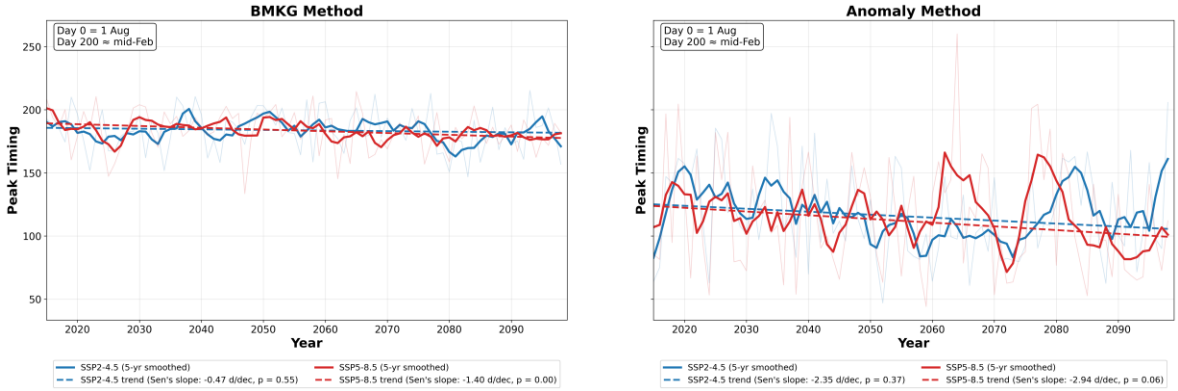


Figure 7. Temporal variation of rainy season peak timing under SSP2-4.5 and SSP5-8.5 scenarios during the 2015–2099 period.

Based on Figure 7, under the BMKG method (left panel), the timing of the rainy season peak fluctuated between approximately 160 and 200 days (early January to mid-February), indicating considerable inter-annual variability. Despite this variability, the Sen's slope analysis showed a decreasing trend of −0.61 days/decade ($p = 0.07$) under SSP2-4.5 and −1.24 days/decade ($p < 0.01$) under SSP5-8.5. The reported negative Sen's slope under SSP5-8.5 (−1.24 days/decade, $p < 0.01$) suggests an apparent shift toward earlier peak timing. However, this interpretation remains provisional because peak timing is a seasonal index that may wrap around the seasonal-cycle boundary. The direction and significance of the trend should be confirmed using an appropriate treatment of the seasonal index and its uncertainty.

Conversely, under the Anomaly method (right panel), the peak timing showed a much larger amplitude of inter-annual variability, fluctuating between approximately 50 and 160 days (late September to early January). The trend analysis revealed a decreasing trend of −1.27 days/decade ($p = 0.14$) under SSP2-4.5 and −2.28 days/decade ($p = 0.02$) under SSP5-8.5. The large interannual variability and SNR values below 1.5 indicate that the projected peak-timing signal under the Anomaly method is relatively weak compared with its variability. This suggests limited robustness of the projected response, although a direct comparison of robustness between methods requires consistent SNR definitions and uncertainty estimates.

When compared to changes in onset and retreat, the peak rainfall parameter showed a more moderate shift. Changes in onset and retreat can affect the length of the rainy season, while peak timing describes the distribution of maximum rainfall within that period. Therefore, even though the rainy season may undergo changes in duration under some scenarios, the period of maximum rainfall occurrence exhibited a slight, statistically significant advance (particularly under SSP5-8.5), although it was largely masked by high inter-annual variability.

© 2026 Dept. of Geophysics Hasanuddin University

Overall, the results suggest that changes in the rainy season peak were characterized by high spatial and inter-annual variation, rather than a uniform systematic shift across the entire basin. The SSP5-8.5 scenario showed greater temporal variability compared to SSP2-4.5, but both scenarios still maintained relatively similar ranges of peak rainfall timing throughout the twenty-first century. These findings suggest that within the study area, climate change may potentially affect the stability of peak rainfall timing, while regional factors and natural atmospheric variability continue to play important roles in determining the temporal dynamics of maximum rainfall.

These findings provide critical insights into the future dynamics of the rainy season over the Brantas Watershed. The projected earlier onset under both scenarios is broadly consistent with previous studies reporting changes in rainy-season timing over parts of the Maritime Continent (Adriat et al., 2025; Hariadi et al., 2022). However, differences in study area, observational references, and seasonal-index definitions should be considered when comparing the magnitude and proposed mechanisms of these changes. However, our findings diverge regarding the rainy season duration. While this study projects a substantial lengthening of duration (+41 to +58 days) based on the BMKG method, previous studies (Wiwoho et al., 2023) reported a relatively stable duration. This discrepancy likely arises from methodological differences. The BMKG threshold method is highly sensitive to the intensification of extreme rainfall, whereas the cumulative Anomaly method captures the relative shift of the seasonal cycle (Dunning et al., 2018).

The stark contrast between these two approaches highlights an important methodological insight: for tropical watersheds characterized by high daily rainfall variability, cumulative Anomaly indices are highly sensitive to daily-scale noise. These findings suggest that the BMKG threshold method may be more suitable for operational applications involving rainy-season duration in the Brantas Watershed, given its stronger historical validation for this parameter. However, method performance varied across parameters and models, so the suitability of either method should be assessed against the specific application and validation metric

Despite these valuable insights, this study has several limitations that should be acknowledged. First, the historical validation was restricted to CMIP6 models and relied on an observational period (2000–2014) that, while independent of the BCCAQ calibration against CHIRPS, still contains inherent uncertainties. Future studies should incorporate pre-2000 observational data to enable a strictly independent validation. Second, the anomaly method exhibited substantial deviations during historical validation, which limits its utility for future projections in this region. Third, the attribution of spatial variations in peak timing to specific local drivers was beyond the scope of this study and requires further dedicated analysis using high-resolution topographic data and large-scale climate indices.

Based on these findings, several recommendations can be made. For water resource managers and agricultural planners in the Brantas Watershed, the projected earlier onset and longer rainy season imply that cropping calendars and reservoir operation strategies may need to be adjusted to accommodate the shifting hydrological cycle. Furthermore, future research should expand the multi-model ensemble by including a wider range of CMIP6 models and integrating large-scale atmospheric dynamics with local geographical factors to fully understand

© 2026 Dept. of Geophysics Hasanuddin University

the spatial heterogeneity of rainy season changes.

Conclusion

This study evaluated projected changes in rainy-season onset, retreat, and duration across the Brantas River Basin under the SSP2-4.5 and SSP5-8.5 scenarios using the BMKG and Anomaly methods. The results revealed differences between the two methods in both the magnitude and direction of projected changes. The BMKG method generally indicated larger changes in seasonal timing and duration, whereas the Anomaly method produced smaller and more variable changes. Trend analysis also identified significant changes in selected parameters, including decreasing anomaly-based onset and duration under SSP5-8.5, as well as increasing BMKG-based duration under the same scenario. These findings highlight the importance of considering methodological differences when interpreting future rainy-season characteristics.

Despite these trends, the strength and spatial consistency of projected changes varied across scenarios and periods. In particular, low signal-to-noise ratios and limited FDR-significant areas for anomaly-based duration indicate substantial uncertainty relative to inter-model variability. Therefore, statistically significant temporal trends should not automatically be interpreted as robust spatial responses across the basin. The findings demonstrate that combining temporal trend analysis with ensemble agreement, signal-to-noise ratios, and spatial significance assessments provides a more comprehensive basis for evaluating future rainy-season changes. This approach can support climate adaptation and water-resource planning in the Brantas River Basin while accounting for uncertainty in future rainfall-season dynamics.

Acknowledgements

The authors gratefully acknowledge the Indonesia Agency for Meteorology, Climatology, and Geophysics (BMKG) for providing operational climate data and for the establishment of the dasarian-based rainy season criteria used in this study. We also thank the Earth System Grid Federation (ESGF) for providing access to CMIP6 model outputs, and the Climate Hazards Group for making the CHIRPS precipitation dataset publicly available.

Author Contribution

Gilang Aulia Herlambang: Conceptualization, data curation, formal analysis, investigation, methodology, validation, visualization, and writing – original draft.
Lalu Muhamad Jaelani: Conceptualization, methodology, project administration, supervision, and writing – review and editing.

Conflict of Interest

The authors declare no conflicts of interest. No financial or personal relationships with other people or organizations have inappropriately influenced or biased the work presented in this study. The funders had no role in the design of the study; in the collection, analyses, or interpretation of data; in the writing of the manuscript; or in the decision to publish the results.

References

Adriat, R., Aprilina, A., Satyawardhana, H., Ihwan, A., & Sutanto, Y. (2025). Identification of variations in the onset of the rainy and dry seasons in Indonesia. *Journal of Bioresources and Environmental Sciences,* 4(2), 102–111. https://doi.org/10.61435/jbes.2025.19960

Bai, L., Shi, C., Li, L., Yang, Y., & Wu, J. (2018). Accuracy of CHIRPS

© 2026 Dept. of Geophysics Hasanuddin University

satellite-rainfall products over mainland China. *Remote Sensing*, 10(3), 362. https://doi.org/10.3390/rs10030362

BBWS Brantas. (2011). *Profil Wilayah Sungai Brantas*. Balai Besar Wilayah Sungai, Direktorat Jenderal Sumber Daya Air, Kementerian Pekerjaan Umum. https://sda.pu.go.id/balai/bbwsbrantas/

Benjamini, Y., & Hochberg, Y. (1995). Controlling the false discovery rate: A practical and powerful approach to multiple testing. *Journal of the Royal Statistical Society: Series B (Methodological), 57*(1), 289–300. https://doi.org/10.1111/j.2517-6161.1995.tb02031.x

BMKG. (2022). *Normal standar iklim 1991–2020 (Buku ZOM 9120)*. Badan Meteorologi, Klimatologi, dan Geofisika. https://iklim.bmkg.go.id/bmkgadmin/storage/buletin/Buku_ZOM9120_versi_cetak.pdf

Bombardi, R. J., Moron, V., & Goodnight, J. S. (2020). Detection, variability, and predictability of monsoon onset and withdrawal dates: A review. *International Journal of Climatology,* 40(2), 641–667. https://doi.org/10.1002/joc.6264

Boucher, O., Servonnat, J., Albright, A. L., Aumont, O., Balkanski, Y., Bastrikov, V., Bekki, S., Bonnet, R., Bony, S., Bopp, L., Braconnot, P., Brockmann, P., Cadule, P., Caubel, A., Cheruy, F., Codron, F., Cozic, A., Cugnet, D., D'Andrea, F., Davini, P., de Lavergne, C., Denvil, S., Deshayes, J., Devilliers, M., Ducharne, A., Dufresne, J.-L., Dupont, E., Éthé, C., Fairhead, L., Falletti, L., Flavoni, S., Foujols, M.-A., Gardoll, S., Gastineau, G., Ghattas, J., Grandpeix, J.-Y., Guenet, B., Guez, L. E., Guilyardi, E., Guimberteau, M., Hauglustaine, D., Hourdin, F., Idelkadi, A., Joussaume, S., Kageyama, M., Khodri, M., Krinner, G., Lebas, N., Levavasseur, G., Lévy, C., Li, L., Lott, F., Lurton, T., Luyssaert, S., Madec, G., Madeleine, J.-B., Maignan, F., Marchand, M., Marti, O., Mellul, L., Meurdesoif, Y., Mignot, J., Musat, I., Ottlé, C., Peylin, P., Planton, Y., Polcher, J., Rio, C., Rochetin, N., Rousset, C., Sepulchre, P., Sima, A., Swingedouw, D., Thiéblemont, R., Traore, A. K., Vancoppenolle, M., Vial, J., Vialard, J., Viovy, N., & Vuichard, N. (2020). Presentation and evaluation of the IPSL-CM6A-LR Climate Model. *Journal of Advances in Modeling Earth Systems*, 12(7), e2019MS002010. https://doi.org/10.1029/2019MS002010

Cannon, A. J., Sobie, S. R., & Murdock, T. Q. (2015). Bias correction of GCM precipitation by quantile mapping: How well do methods preserve changes in quantiles and extremes? *Journal of Climate,* 28(17), 6938–6959. https://doi.org/10.1175/JCLI-D-14-00754.1

Chen, C.-A., Hsu, H- H., & Liang, H.-C. (2021). Evaluation and comparison of CMIP6 and CMIP5 model performance in simulating the seasonal extreme precipitation in the Western North Pacific and East Asia. *Weather and Climate Extremes*, 31, 100303. https://doi.org/10.1016/j.wace.2021.100303

Dinku, T., Funk, C., Peterson, P., Maidment, R., Tadesse, T., Gadain, H., & Ceccato, P. (2018). Validation of the CHIRPS satellite rainfall estimates over eastern Africa. *Quarterly Journal of the Royal Meteorological Society*, 144, 292–312. https://doi.org/10.1002/qj.3244

Dunne, J. P., Horowitz, L. W., Adcroft, A. J., Ginoux, P., Held, I. M., John, J. G., Krasting, J. P., Malyshev, S., Naik, V., Paulot, F., Shevliakova, E., Stock,

© 2026 Dept. of Geophysics Hasanuddin University

C. A., Winton, M., Zadeh, N., Balaji, V., Blanton, C., Dunne, K. A., Dupuis, C., Durachta, J., Dupuis, R., Gauthier, P. P. G., Griffies, S. M., Guo, H., Hallberg, R. W., Harrison, M., He, J., Hurlin, W., McHugh, C., Menzel, R., Milly, P. C. D., Nikonov, S., Paynter, D. J., Ploshay, J., Radhakrishnan, A., Rand, K., Reichl, B. G., Robinson, T., Schwarzkopf, D. M., Sentman, L. T., Underwood, S., Vahlenkamp, H., Winton, M., Wittenberg, A. T., Wyman, B., Zeng, Y., & Zhao, M. (2020). The GFDL Earth System Model Version 4.1 (GFDL-ESM4.1): Overall coupled model description and simulation characteristics. *Journal of Advances in Modeling Earth Systems*, 12(11), e2019MS002015. https://doi.org/10.1029/2019MS002015

Döscher, R., Acosta, M., Alessandri, A., Anthoni, P., Arsouze, T., Bergman, T., Bernardello, R., Boussetta, S., Caron, L.-P., Carver, G., Castrillo, M., Catalano, F., Cvijanovic, I., Davini, P., Dekker, E., Doblas-Reyes, F. J., Docquier, D., Echevarria, P., Fladrich, U., Fuentes-Franco, R., Gröger, M., von Hardenberg, J., Hieronymus, J., Karami, M. P., Keskinen, J.-P., Koenigk, T., Makkonen, R., Massonnet, F., Ménégoz, M., Miller, P. A., Moreno-Chamarro, E., Nieradzik, L., van Noije, T., Nolan, P., O'Donnell, D., Ollinaho, P., van den Oord, G., Ortega, P., Tintó Prims, O., Ramos, A., Reerink, T., Rousset, C., Ruprich-Robert, Y., Le Sager, P., Schmith, T., Schrödner, R., Serva, F., Sicardi, V., Sloth Madsen, M., Smith, B., Tian, T., Tourigny, É., Uotila, P., Vancoppenolle, M., Wang, S., Wårlind, D., Willén, U., Wyser, K., Yang, S., Yepes-Arbós, X., & Zhang, Q. (2022). The EC-Earth3 Earth system model for the Coupled Model Inter-comparison Project 6. *Geoscientific Model Development*, 15(7), 2975–3020. https://doi.org/10.5194/gmd-15-2973-2022

Dunning, C. M., Allan, R. P., & Black, E. (2017). Identification of deficiencies in seasonal rainfall simulated by CMIP5 climate models. *Environmental Research Letters,* 12, 114001. https://doi.org/10.1088/1748-9326/aa869e

Dunning, C. M., Black, E., & Allan, R. P. (2018). Later wet seasons with more intense rainfall over Africa under future climate change. *Journal of Climate*, 31(23), 9719–9738. https://doi.org/10.1175/JCLI-D-18-0102.1

Eyring, V., Bony, S., Meehl, G. A., Senior, C. A., Stevens, B., Stouffer, R. J., & Taylor, K. E. (2016). Overview of the Coupled Model Intercomparison Project Phase 6 (CMIP6) experimental design and organization. *Geoscientific Model Development,* 9(5), 1937–1958. https://doi.org/10.5194/gmd-9-1937-2016

Ferijal, T., Mechram, S., Fauzi, A., & Ferdiansyah, T. (2025). Performance analysis of satellite-derived precipitation data in Aceh, Indonesia. *International Journal of Geoinformatics*, 21(7), 1–15. https://doi.org/10.52939/ijg.v21i7.4311

Funk, C., Peterson, P., Landsfeld, M., Pedreros, D., Verdin, J., Shukla, S., Husak, G., Rowland, J., Harrison, L., Hoell, A., & Michaelsen, J. (2015). The climate hazards infrared precipitation with stations—a new environmental record for monitoring extremes. *Scientific Data,* 2, 150066. https://doi.org/10.1038/sdata.2015.66

Gebrechorkos, S. H., Leyland, J., Slater, L., Wortmann, M., Ashworth, P. J., Bennett, G. L., Boothroyd, R., Cloke, H., Delorme, P., Griffith, H., Hardy,

© 2026 Dept. of Geophysics Hasanuddin University

R., Hawker, L., McLelland, S., Neal, J., Nicholas, A., Parsons, D. R., Tatem, A. J., Vahidi, E., & Darby, S. E. (2023). A high-resolution daily global dataset of statistically downscaled CMIP6 models for climate impact analyses. *Scientific Data,* 10, 611. https://doi.org/10.1038/s41597-023-02528-x

Gupta, R., Prakash, P., & Chembolu, V. (2025). Multi criteria evaluation of downscaled CMIP6 models in predicting precipitation extremes. *Atmospheric Research*, 315, 107921. https://doi.org/10.1016/j.atmosres.2025.107921

Hajima, T., Watanabe, M., Yamamoto, A., Tatebe, H., Noguchi, M. A., Abe, M., Ohgaito, R., Ito, A., Yamazaki, D., Okajima, H., Ito, A., Takata, K., Ogochi, K., Watanabe, S., & Kawamiya, M. (2020). Develop-ment of the MIROC ES2L Earth system model and the evaluation of biogeochemical processes and feedbacks. *Geoscientific Model Development*, 13(5), 2197–2244. https://doi.org/10.5194/gmd-13-2197-2020

Hamed, K. H., & Rao, A. R. (1998). A modified Mann-Kendall trend test for autocorrelated data. *Journal of Hydrology,* 204(1–4), 182–196. https://doi.org/10.1016/S0022-1694(97)00125-X

Hariadi, M. H., van der Schrier, G., Steeneveld, G.-J., Sopaheluwakan, A., Tank, A. K., Roberts, M. J., Moine, M.-P., Bellucci, A., Senan, R., Tourigny, E., & Putrasahan, D. (2022). Evaluation of onset, cessation and seasonal precipitation of the Southeast Asia rainy season in CMIP5 regional climate models and HighResMIP global climate models. *International Journal of Climatology,* 42(5), 3007–3024. https://doi.org/10.1002/joc.7404

Herlambang, G. A., & Jaelani, L. M. (2026). Assessing future precipitation patterns in the Brantas River Basin through downscaling of CMIP6 GCMs. *IOP Conference Series: Earth and Environmental Science,* 1607(1), 012036. https://doi.org/10.1088/1755-1315/1607/1/012036

IPCC. (2021). *Climate Change 2021: The Physical Science Basis. Contribution of Working Group I to the Sixth Assessment Report of the Intergovernmental Panel on Climate Change*. Intergovernmental Panel on Climate Change. Cambridge University Press. https://doi.org/10.1017/9781009157896

IPCC. (2023). *Climate Change 2023: Synthesis Report. Contribution of Working Groups I, II and III to the Sixth Assessment Report of the Intergovernmental Panel on Climate Change* (H. Lee & J. Romero, Eds.). Intergovernmental Panel on Climate Change. https://doi.org/10.59327/IPCC/AR6-9789291691647

Iqbal, Z., Shahid, S., Ahmed, K., Ismail, T., Ziarh, G. F., Chung, E.-S., & Wang, X. (2021). Evaluation of CMIP6 GCM rainfall in mainland Southeast Asia. *Atmospheric Research,* 254, 105525. https://doi.org/10.1016/j.atmosres.2021.105525

Kurniadi, A., Weller, E., Kim, Y.-H., & Min, S.-K. (2023). Evaluation of Coupled Model Intercomparison Project Phase 6 model-simulated extreme precipitation over Indonesia. *International Journal of Climatology,* 43(1), 174–196. https://doi.org/10.1002/joc.7744

Kurniadi, A., Weller, E., Salmond, J., & Aldrian, E. (2024). Future projections of extreme rainfall events in Indonesia. International *Journal of*

© 2026 Dept. of Geophysics Hasanuddin University

Climatology, 44(1), 160–182. https://doi.org/10.1002/joc.8321

Kwawuvi, D., Mama, D., Agodzo, S. K., Hartmann, A., Larbi, I., Bessah, E., Abraham, T., Dotse, S.-Q., & Limantol, A. M. (2022). An investigation into the future changes in rainfall onset, cessation and length of rainy season in the Oti River Basin, West Africa. *Modeling Earth Systems and Environment,* 8(4), 5077–5095. https://doi.org/10.1007/s40808-022-01410-w

Lafferty, D. C., & Sriver, R. L. (2023). Downscaling and bias-correction contribute considerable uncertainty to local climate projections in CMIP6. *npj Climate and Atmospheric Science,* 6, 158. https://doi.org/10.1038/s41612-023-00486-0

Liebmann, B., Camargo, S. J., Seth, A., Marengo, J. A., Carvalho, L. M. V., Allured, D., Fu, R., & Vera, C. S. (2007). Onset and end of the rainy season in South America in observations and the ECHAM 4.5 atmospheric general circulation model. *Journal of Climate,* 20(10), 2037–2050. https://doi.org/10.1175/JCLI4122.1

Liu, S., Raghavan, S. V., Nguyen, N. S., & Ona, B. J. (2022). Evaluations of the sixth phase of Coupled Model Intercomparison Project model performance on precipitation over Southeast Asia based on the moisture budget. *International Journal of Climatology*, 42(14), 7087–7102. https://doi.org/10.1002/joc.7631

Liu, S., Raghavan, S. V., Ona, B. J., & Nguyen, N. S. (2023). Bias evaluation in rainfall over Southeast Asia in CMIP6 models. *Journal of Hydrology*, 621, 129593. https://doi.org/10.1016/j.jhydrol.2023.129593

Long, Y., Zheng, M., He, H., & Yan, S. (2023). Interannual variabilities in the onset and demise of rainy season: Implications for water management. *Water Resources Management,* 37(12), 4933–4948. https://doi.org/10.1007/s11269-023-03589-8

Moon, S., & Ha, K.-J. (2020). Future changes in monsoon duration and precipitation using CMIP6. *npj Climate and Atmospheric Science,* 3, 45. https://doi.org/10.1038/s41612-020-00151-w

Mulsandi, A., Koesmaryono, Y., Hidayat, R., Faqih, A., & Sopaheluwakan, A. (2024). Detecting Indonesian monsoon signals and related features using space–time singular value decomposition (SVD). *Atmosphere*, 15(2), 187. https://doi.org/10.3390/atmos15020187

O'Neill, B. C., Tebaldi, C., van Vuuren, D. P., Eyring, V., Friedlingstein, P., Hurtt, G., Knutti, R., Kriegler, E., Lamarque, J.-F., Lowe, J., Meehl, G. A., Moss, R., Riahi, K., & Sanderson, B. M. (2016). The Scenario Model Intercomparison Project (ScenarioMIP) for CMIP6. *Geoscientific Model Development,* 9(9), 3461–3482. https://doi.org/10.5194/gmd-9-3461-2016

Paredes-Trejo, F. J., Barbosa, H. A., & Kumar, T. V. L. (2017). Validating CHIRPS-based satellite precipitation estimates in Northeast Brazil. *Journal of Arid Environments*, 139, 26–40. https://doi.org/10.1016/j.jaridenv.2016.12.009

Pimonsree, S., Kamworapan, S., Gheewala S. H., Thongbhakdi, A., & Prueksakorn, K. (2023). Evaluation of CMIP6 GCMs for simulating precipitation over Thailand and Indonesia. *Atmospheric Research, 282*, 106522. https://doi.org/10.1016/j.atmosres.2022.106522

Prasetya, R. P., Djuhana, D., Saputro, A. H. H., & Permana, D. S. (2026).

© 2026 Dept. of Geophysics Hasanuddin University

Evaluation and ranking of NEX-GDDP-CMIP6 models based on monthly precipitation climatology over Indonesia. *Frontiers in Climate,* 8, 1748663. https://doi.org/10.3389/fclim.2026.1748663

Raghavan, S. V., Hur, J., & Liong, S.-Y. (2018). Evaluations of NASA NEX-GDDP data over Southeast Asia: Present and future climates. *Climatic Change*, 148, 503–518. https://doi.org/10.1007/s10584-018-2213-3

Rahmawati, N., & Lubczynski, M. W. (2018). Validation of satellite daily rainfall estimates in complex terrain of Bali Island, Indonesia. *Theoretical and Applied Climatology*, 134, 513–532. https://doi.org/10.1007/s00704-017-2290-7

Riahi, K., van Vuuren, D. P., Kriegler, E., Edmonds, J., O'Neill, B. C., Fujimori, S., Bauer, N., Calvin, K., Dellink, R., Fricko, O., Lutz, W., Popp, A., Cuaresma, J. C., KC, S., Leimbach, M., Jiang, L., Kram, T., Rao, S., Emmerling, J., Ebi, K., & Tavoni, M. (2017). The Shared Socioeconomic Pathways and their energy, land use, and greenhouse gas emissions implications: An overview. *Global Environmental Change, 42*, 153–168. https://doi.org/10.1016/j.gloenvcha.2016.05.009

Seland, Ø., Bentsen, M., Olivié, D., Toniazzo, T., Gjermundsen, A., Graff, L. S., Debernard, J. B., Gupta, A. K., He, Y.-C., Kirkevåg, A., Schwinger, J., Tjiputra, J., Aas, K. S., Bethke, I., Fan, Y., Griesfeller, J., Grini, A., Guo, C., Ilicak, M., Karset, I. H. H., Landgren, O., Liakka, J., Moseid, K. O., Nummelin, A., Spensberger, C., Tang, H., Zhang, Z., Heinze, C., Iversen, T., & Schulz, M. (2020). Overview of the Norwayn Earth System Model (NorESM2) and key climate response of CMIP6 simulations. *Geoscientific Model Development*, 13(12), 6165–6200. https://doi.org/10.5194/gmd-13-6165-2020

Shakeel, M., Abbas, H., Ali, Z., Tariq, A., Almazroui, M., & Kader, S. (2025). A novel framework for future drought characterization under ranked-based subset selection and weighted aggregative multi-modal ensemble of global climate models. *Journal of Environmental Management*, 392, 126692. https://doi.org/10.1016/j.jenvman.2025.126692

Shrestha, B. B., Rasmy, M., Ushiyama, T., Acierto, R. A., Kawamoto, T., Fujikane, M., Shinya, T., & Kubota, K. (2025). Assessment of future risk of agricultural crop production under climate and social changes scenarios: A case of the Solo River basin in Indonesia. *Journal of Flood Risk Management,* 18(1), e13052. https://doi.org/10.1111/jfr3.13052

Sudarman, G. G., Hadi, T. W., Ningsih, N. S., Sopaheluwakan, A., Syahputra, M. R., & Marpaung, F. (2024). Nonstationary changes in annual rainfall over Indonesia's maritime continent. *Advances in Meteorology*, 2024, 9392844. https://doi.org/10.1155/2024/9392844

Supari, Tangang, F., Salimun, E., Aldrian, E., Sopaheluwakan, A., & Juneng, L. (2018). ENSO modulation of seasonal rainfall and extremes in Indonesia. *Climate Dynamics*, 51, 2559–2580. https://doi.org/10.1007/s00382-017-4028-8

Supari, S., Tangang, F., Juneng, L., Cruz, F., Chung, J. X., Ngai, S. T., Salimun, E., Mohd, M. S. F., Santisirisomboon, J., Singhruck, P., PhanVan, T., Ngo-Duc, T., Narisma, G., Aldrian, E., Gunawan, D., & Sopaheluwakan, A. (2020). Multi-model projections of precipitation extremes in Southeast Asia based on CORDEX-Southeast

© 2026 Dept. of Geophysics Hasanuddin University

Asia simulations. *Environmental Research,* 184, 109350. https://doi.org/10.1016/j.envres.2020.109350

Taguela, T. N., Raji, I., Akinsanola, A. A., Singhai, P., Adeyeri, O. E., Wainwright, C. M., & Barimalala, R. (2026). Impacts of 1.5°C and 2.0°C global warming on the onset, cessation, and length of the rainy season in global land monsoon regions. *Advances in Atmospheric Sciences,* 43, 87–102. https://doi.org/10.1007/s00376-025-4386-9

Tebaldi, C., Debeire, K., Eyring, V., Fischer, E., Fyfe, J., Friedlingstein, P., Knutti, R., Lowe, J., O'Neill, B., Sanderson, B., van Vuuren, D., Riahi, K., Meinshausen, M., Nicholls, Z., Tokarska, K. B., Hurtt, G., Kriegler, E., Lamarque, J.-F., Meehl, G., Moss, R., Bauer, S. E., Boucher, O., Brovkin, V., Byun, Y.-H., Dix, M., Gualdi, S., Guo, H., John, J. G., Kharin, S., Kim, Y.H., Koshiro, T., Ma, L., Olivié, D., Panickal, S., Qiao, F., Rong, X., Rosenbloom, N., Schupfner, M., Séférian, R., Sellar, A., Semmler, T., Shi, X., Song, Z., Steger, C., Stouffer, R., Swart, N., Tachiiri, K., Tang, Q., Tatebe, H., Voldoire, A., Volodin, E., Wyser, K., Xin, X., Yang, S., Yu, Y., & Ziehn, T. (2021). Climate model projections from the Scenario Model Intercomparison Project (ScenarioMIP) of CMIP6. *Earth System Dynamics*, 12(1), 253-293. https://doi.org/10.5194/esd-12-253-2021

Werner, A. T., & Cannon, A. J. (2016). Hydrologic extremes – an intercomparison of multiple gridded statistical downscaling methods. *Hydrology and Earth System Sciences,* 20(4), 1483–1508. https://doi.org/10.5194/hess-20-1483-2016

Wiwoho, B. S., Astuti, I. S., Alfarizi, I. A. G., & Sucahyo, H. R. (2021). Validation of three daily satellite rainfall products in a humid tropic watershed, Brantas, Indonesia: Implications to land characteristics and hydrological modelling. *Hydrology*, 8(4), 154. https://doi.org/10.3390/hydrology8040154

Wiwoho, B. S., Astuti, I. S., Purwanto, P., Deffinika, I., Alfarizi, I. A. G., Sucahyo, H. R., Gusti, R., Herwanto, M. T., & Herlambang, G. A. (2023). Assessing long-term rainfall trends and changes in a tropical watershed Brantas, Indonesia: An approach for quantifying the agreement among satellite-based rainfall data, ground rainfall data, and small-scale farmers questionnaires. *Natural Hazards,* 117, 2535–2562. https://doi.org/10.1007/s11069-023-05969-0

Wiwoho, B. S., Dargusch, P., & Astuti, I. S. (2025). An analysis of rainfall variability and its association with agricultural productivity in the Brantas River Basin, Indonesia: Insights from a 26-year analysis. *Ecohydrology & Hydrobiology,* 25(4), 100674. https://doi.org/10.1016/j.ecohyd.2025.100674

Yulizar, Y., & Asdak, C. (2025). The joint variation of temperature and precipitation across Indonesia: A seasonal and regional analysis. *Theoretical and Applied Climatology,* 156(11), Article 624. https://doi.org/10.1007/s00704-025-05872-7

Zabihi, O., & Ahmadi, A. (2024). Multi-criteria evaluation of CMIP6 precipitation and temperature simulations over Iran. Journal of Hydrology: Regional Studies, 52, 101707. https://doi.org/10.1016/j.ejrh.2024.101707

© 2026 Dept. of Geophysics Hasanuddin University